

Effect of flow field design on the performance of elevated-temperature polymer electrolyte fuel cells

Puneet K. Sinha^{1,2}, Chao-Yang Wang^{1,2,*},† and Uwe Beuscher³

¹*Electrochemical Engine Center (ECEC), The Pennsylvania State University, University Park, PA 16802, U.S.A.*

²*Department of Mechanical and Nuclear Engineering, The Pennsylvania State University, University Park, PA 16802, U.S.A.*

³*Gore Fuel Cell Technologies, W.L. Gore & Associates, Inc., 201 Airport Road, Elkton, MD 21921, U.S.A.*

SUMMARY

In our previous work, operation of polymer electrolyte fuel cell (PEFC) at 95°C was investigated in detail and it was found that dry operation of PEFC at elevated temperatures makes the parallel flow field design a viable design option for high temperature applications such as for automobiles. In this work, a three-dimensional, non-isothermal PEFC model is used to compare the performance of a 25 cm² fuel cell with serpentine and parallel flow field design operated at 95°C under various inlet humidity conditions. Numerical results show that the parallel flow field provides better and more uniformly distributed performance over the whole active area which makes the parallel flow field a better design compared to the serpentine flow field for PEFCs operated at elevated temperature and low inlet relative humidity. Copyright © 2006 John Wiley & Sons, Ltd.

KEY WORDS: 95°C operation; polymer electrolyte fuel cell; non-isothermal model; parallel and serpentine flow field design

1. INTRODUCTION

Polymer electrolyte fuel cells (PEFC) are considered the most promising alternative power plant for transportation because of their high efficiency, low emissions, low operating temperature, and low noise. Much efforts has been expended in last decade upon development of numerical models with more physical complexities to address electrochemical and transport phenomena involved in a fuel cell and occurring at disparate length and time scales. In the last 5 years, computational fluid dynamics (CFD)-based model were developed with the coupling of

*Correspondence to: Chao-Yang Wang, Department of Mechanical and Nuclear Engineering, The Pennsylvania State University, University Park, PA 16802, U.S.A.

†E-mail: cxw31@psu.edu

Contract/grant sponsor: W.L. Gore & Associates Inc.

multi-dimensional transport phenomena with electrochemical kinetics and charge transport to provide a comprehensive understanding of fuel cell dynamics. For CFD modelling of PEFC, one can refer to Wang (2004) and references therein.

PEFC performance is largely influenced by the flow field design. Over the years, several flow field designs were proposed and the effect of the flow field design on PEFC performance was investigated in detail (Mench *et al.*, 2001; Pasaogullari and Wang, 2002; Glandt *et al.*, 2002; Wang and Wang, 2006). Two flow field designs are commonly used in practice: the serpentine flow field and the parallel flow field. The parallel flow field incurs less pressure drop between inlet and outlet of the gas channels in comparison to the serpentine flow field. The parallel flow field also provides a more uniform distribution of reactant over the whole active area. A main disadvantage of the parallel flow field design, however, is clogging of the gas channel by liquid water. Once a channel becomes clogged, the active area under it becomes inactive for rest of the operation, whereas the serpentine flow field can flush out liquid water more easily via high gas flow rate and gas bypassing through gas diffusion layer (GDL) is possible as well. Typically, this drawback of parallel flow field design restricts their use in PEFC.

Sinha *et al.* (2006) investigated species, heat and charge transport in a PEFC operated at 95°C. They identified better oxygen reduction reaction (ORR) kinetics, low membrane hydration and dominant oxygen depletion as main characteristics of cell operation at this elevated temperature. They also showed that dry operation of cell results in a relative humidity (RH) less than unity in both anode and cathode gas channels. This eliminates the possibility of channel clogging and makes the parallel flow field an attractive design option for high-temperature applications such as for automobiles. The comparison of elevated-temperature PEFC performance with parallel flow field design and serpentine flow field design can provide a better assessment of the feasibility of the parallel flow field as a design option for high-temperature applications.

The main objective of this paper is to provide a detailed comparison of the PEFC performance operated at 95°C with parallel and serpentine flow field designs using the three-dimensional electrochemical reaction-transport-thermal coupled PEFC model presented by Sinha *et al.* (2006). We aim to compare not only the cell performance in terms of cell voltage, but also the current density distribution and other key parameters over the whole active area for the two flow field designs under various operating conditions.

2. NUMERICAL MODEL

The present three-dimensional, non-isothermal, electrochemical and transport fully coupled PEFC model is developed based on the previous work of Um *et al.* (2000), Meng and Wang (2004a) and Ju *et al.* (2005a) and has been described in detail by Sinha *et al.* (2006). Thus, only a brief summary of the model assumptions is repeated here:

1. Ideal gas mixtures;
2. Isotropic and homogenous electrode, catalyst layers and membrane;
3. Incompressible and laminar flow due to small pressure gradient and flow velocities; and
4. Single-phase assumption for water transport.

Assumption 4 is valid under the condition that the liquid saturation within the GDL is low or liquid droplets are small and dispersed in gas to form a mist flow. The PEFC model is

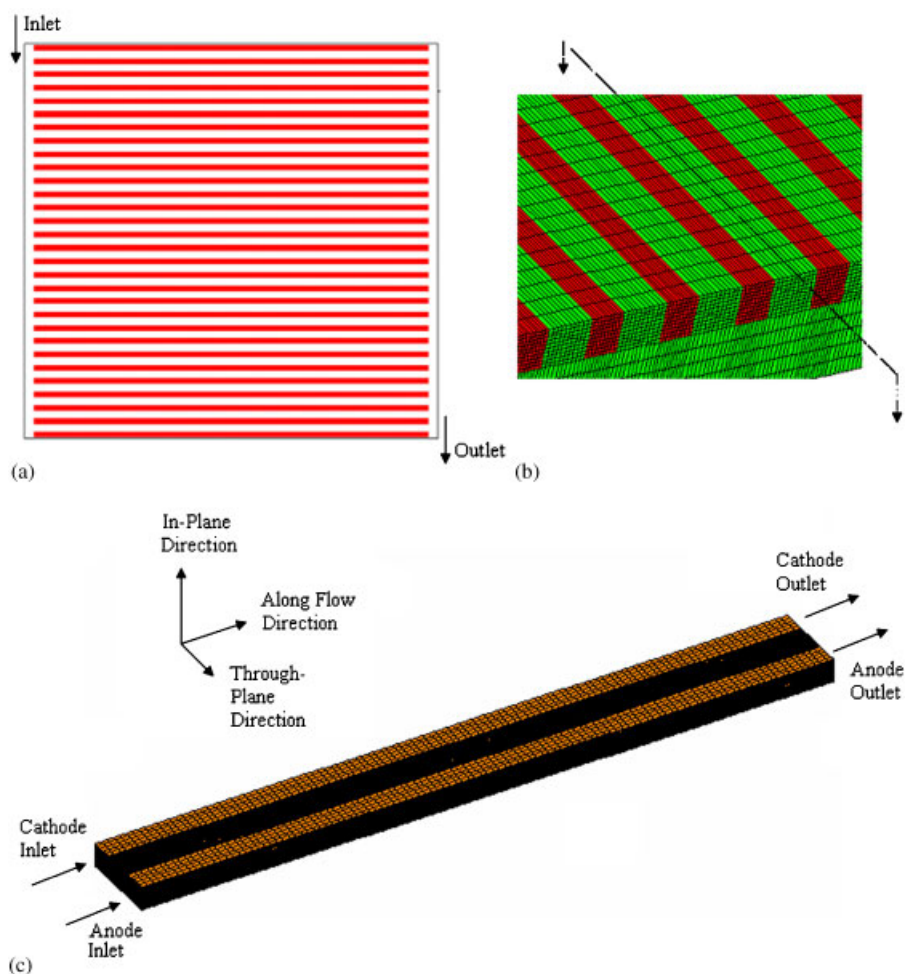


Figure 2. (a) Schematic of parallel flow field for 25 cm² cell; (b) cutting plane for a single-channel unit cell; and (c) schematic of unit cell cut out of cell with parallel flow field.

to a single-channel unit cell, cut out from the 25 cm² cell with parallel flow field as shown in Figure 2(b), having the same dimensions in the through plane and along the flow direction with a periodic extension in the in-plane direction. The single-channel unit cell is shown in Figure 2(c).

Based on the grid independence study of Meng and Wang (2004b), roughly 2.0 million computational cells are applied to the three-pass serpentine flow field geometry and roughly 94 000 computational cells to the single-channel geometry. This model requires about 270 s per iteration on a 8 PC cluster (1.4 GHz) for the three-pass serpentine geometry and about 15 s per iteration on a single PC (2 GHz) for the single-channel geometry.

3. RESULTS AND DISCUSSION

The present PEFC model is used to study the performance of a 25 cm² three-pass serpentine flow field PEFC and a 25 cm² parallel flow field PEFC operated at 95°C. Both fuel cells have the same dimensions and parameters except for the flow field design. The predicted cell voltages for two current densities (0.8 and 1.6 A cm⁻²) and at two different inlet RH (30% at both anode and cathode inlets and 50% at anode inlet and 0% at cathode inlet) are listed in Table I. All the geometric parameters are tabulated in Table II. For all cases, the inlet pressure on both anode and cathode was 270 KPa and the anode and cathode stoichiometry ratios were set to 1.3 and 2.0, respectively. In addition, the temperatures of all external surfaces were maintained at 95°C, allowing the application of the isothermal boundary condition in the model. A contact resistance of 50 mΩ cm² is applied in all the numerical simulations to account for all the interfacial resistances within the fuel cell. All material properties and the functional relationships used in the simulations are listed in Table III and IV respectively. For simplicity, three-pass serpentine flow field will be referred as serpentine flow field in the following discussion.

Table I. Performance study with two flow field designs for 25 cm² PEFC and 95°C operation.

Cases	$\xi_{\text{anode}}/\xi_{\text{cathode}}$	RH _{anode} /RH _{cathode} (%/%)	Current density (A cm ⁻²)	Cell voltage (V)	
				(Parallel Flow Field)	(Serpentine Flow Field)
1	1.3/2.0	30/30	0.8	0.685	0.680
2	1.3/2.0	50/0	0.8	0.630	0.625
3	1.3/2.0	30/30	1.6	0.480	0.474
4	1.3/2.0	50/0	1.6	0.422	0.400

Table II. Cell design parameters.

Description	Value
Anode/cathode macro gas diffusion layer thickness	0.230 mm
Anode/cathode micro gas diffusion layer thickness	0.060 mm
Anode/cathode catalyst layer thickness	0.010 mm
Anode/cathode gas channel depth	0.846 mm
Anode/cathode bipolar plate thickness	1.59 mm
Height of cell in the in-plane direction (for 25 cm ² geometry)	47.695 mm
Height of cell in the in-plane direction (for single-channel geometry)	1.621 mm
Membrane width (Gore-select [®])	0.018 mm
Porosity of anode/cathode macro gas diffusion layer, ε_{GDL}	0.7
Porosity of anode/cathode micro gas diffusion layer, ε_{MPL}	0.5
Porosity of anode/cathode catalyst layer, ε_{cat}	0.6
Tortuosity of porous layer for species diffusion, ζ	1.2
Tortuosity of catalyst layer for ionic conductivity, ζ_{k}	1.25
Volume fraction of ionomer in anode/cathode catalyst layer, ε_{mc}	0.26
Permeability of anode/cathode macro gas diffusion layers, K_{GDL}	4.0×10^{-12} m ²
Permeability of anode/cathode micro gas diffusion layers, K_{MPL}	2.0×10^{-15} m ²

Table III. Kinetics, physical, transport and thermal properties.

Description	References	Value
Exchange current density \times specific reaction surface in anode side, $ai_{0,a}^{\text{ref}}$	Ju <i>et al.</i> (2005b)	$1.0 \times 10^9 \text{ Am}^{-3}$
Exchange current density \times specific reaction surface in cathode side, $ai_{0,c}^{\text{ref}}$	Sinha <i>et al.</i> (2006)	$2.0 \times 10^4 \text{ Am}^{-3}$
Reference hydrogen molar concentration, $c_{\text{H}_2,\text{ref}}$	Ju <i>et al.</i> (2005b)	40.88 mol m^{-3}
Reference oxygen molar concentration, $c_{\text{O}_2,\text{ref}}$	Ju <i>et al.</i> (2005b)	40.88 mol m^{-3}
Anodic and cathodic transfer coefficients for hydrogen oxidation reaction		$\alpha_a = \alpha_c = 1$
Cathodic transfer coefficient for oxygen reduction reaction		$\alpha_c = 1$
Dry membrane density, $\rho_{\text{dry,mem}}$	Courtesy Gore	2000 kg m^3
Equivalent weight of membrane, EW	Courtesy Gore	1.1 kg mol^{-1}
H ₂ diffusivity in membrane, $D_{\text{H}_2}^c$	Ju <i>et al.</i> (2005b)	$2.59 \times 10^{-10} \text{ m}^2 \text{ s}^{-1}$
O ₂ diffusivity in membrane, $D_{\text{O}_2}^c$	Ju <i>et al.</i> (2005b)	$1.22 \times 10^{-10} \text{ m}^2 \text{ s}^{-1}$
H ₂ diffusivity in the anode gas channel, $D_{0,\text{H}_2,a}$	Bird <i>et al.</i> (1960)	$1.1028 \times 10^{-4} \text{ m}^2 \text{ s}^{-1}$
H ₂ O diffusivity in the anode gas channel, $D_{0,w,a}$	Bird <i>et al.</i> (1960)	$1.1028 \times 10^{-4} \text{ m}^2 \text{ s}^{-1}$
O ₂ diffusivity in the cathode gas channel, $D_{0,\text{O}_2,c}$	Bird <i>et al.</i> (1960)	$3.2348 \times 10^{-5} \text{ m}^2 \text{ s}^{-1}$
H ₂ O diffusivity in the cathode gas channel, $D_{0,w,c}$	Bird <i>et al.</i> (1960)	$7.35 \times 10^{-5} \text{ m}^2 \text{ s}^{-1}$
Thermal conductivity of hydrogen (H ₂), k_{H_2}	Bird <i>et al.</i> (1960)	0.2040 W mK^{-1}
Thermal conductivity of oxygen (O ₂), k_{O_2}	Bird <i>et al.</i> (1960)	0.0296 W mK^{-1}
Thermal conductivity of water vapour, k_w	Bird <i>et al.</i> (1960)	0.0237 W mK^{-1}
Thermal conductivity of nitrogen (N ₂), k_{N_2}	Bird <i>et al.</i> (1960)	0.0293 W mK^{-1}
Thermal conductivity of membrane, k_{mem}	Courtesy Gore	0.950 W mK^{-1}
Thermal conductivity of macro gas diffusion layer, k_{GDL}	Courtesy Gore	1.19 W mK^{-1}
Thermal conductivity of micro gas diffusion layer, k_{MPL}	Courtesy Gore	1.19 W mK^{-1}
Electronic conductivity of macro gas diffusion layer, σ_{GDL}	Courtesy Gore	6666.67 S m^{-1}
Electronic conductivity of micro gas diffusion layer, σ_{MPL}	Courtesy Gore	200 S m^{-1}
Electronic conductivity of catalyst layer, σ_{cat}	Courtesy Gore	200 S m^{-1}
Electronic conductivity of bipolar plate, σ_{BP}	Courtesy Gore	20000 S m^{-1}

As shown in Table I, the parallel flow field design provides higher cell voltage in comparison to the serpentine flow field design. Although the difference in cell voltage is small (within 5 mV) for 0.8 A cm^{-2} , it is large for 1.6 A cm^{-2} average current density. In addition to comparing the net performance for these two designs it is also necessary to investigate the uniformity of the distribution of performance over the whole active area. A more uniform distribution indicates a better utilization of the whole active area and is preferred. For the present study the distributions of water activity, ionic conductivity and current density over the whole active area are chosen representative for the cell performance.

Figures 3 and 4 show the distributions of water activity in the middle section of the membrane for serpentine and parallel flow field designs at 0.8 A cm^{-2} average current density. Water activity in the membrane increases along the flow direction due to water production in the cathode catalyst layer. As seen from the Figures 3 and 4, the tortuous serpentine flow field provides better water retention at the U-turns and, hence, results in higher water activity at these locations. Whereas, due to the independent functionality of each channel in the parallel flow field, the variation of water activity is equal under each channel and results in a periodic distribution of water activity over the whole active area. Membranes are better hydrated for 1.6 A cm^{-2} average current density, as shown in Figures 5 and 6. As shown in Figures 5 and 6,

Table IV. Constitutive relationships used in the model.

Quantity	Functional Relationship	Reference
Diffusivity of gases in channels	$D_k = D_0 \left(\frac{T}{T_0}\right)^{3/2} \left(\frac{P_0}{P}\right)$ for gas channel	Bird <i>et al.</i> (1960)
Water content in membrane	$\lambda = \begin{cases} 0.043 + 17.81a - 39.85a^2 + 36.0a^3 & \text{for } 0 < a \leq 1 \\ 14 + 1.4(a - 1) & \text{for } 1 < a \leq 3 \end{cases}$	Springer <i>et al.</i> (1991)
Ionic conductivity of Nafion membrane	$\kappa_{\text{mem}} = (0.5139\lambda - 0.326) \exp \left[1268 \left(\frac{1}{303} - \frac{1}{T} \right) \right]$	Springer <i>et al.</i> (1991)
Ionic conductivity of Gore-Select® membrane	$\kappa_{\text{mem}}^{\text{eff}} = \frac{1}{2} \kappa_{\text{mem}} = \frac{1}{2} (0.5139\lambda - 0.326) \exp \left[1268 \left(\frac{1}{303} - \frac{1}{T} \right) \right]$	Ju <i>et al.</i> (2005 b)
Water diffusivity in Nafion membrane	$D_{w,\text{mem}} = \begin{cases} 2.692661843 \times 10^{-10} & \text{for } \lambda \leq 2 \\ \{0.87(3 - \lambda) + 2.95(\lambda - 2)\} \times 10^{-10} e^{(7.9728 - 2416/T)} & \text{for } 2 < \lambda \leq 3 \\ \{2.95(4 - \lambda) + 1.642454(\lambda - 3)\} \times 10^{-10} e^{(7.9728 - 2416/T)} & \text{for } 3 < \lambda \leq 4 \\ \{2.563 - 0.33\lambda + 0.0264\lambda^2 - 0.000671\lambda^3\} \times 10^{-10} e^{(7.9728 - 2416/T)} & \text{for } \lambda > 4 \end{cases}$	Springer <i>et al.</i> (1991)
Water diffusivity in Gore-Select® membrane	$D_{w,\text{mem}}^{\text{eff}} = \frac{1}{2} D_{w,\text{mem}}$	Ju <i>et al.</i> (2005 b)
Electro-osmotic drag	$n_d = 2.5\lambda/22$	Springer <i>et al.</i> (1991)

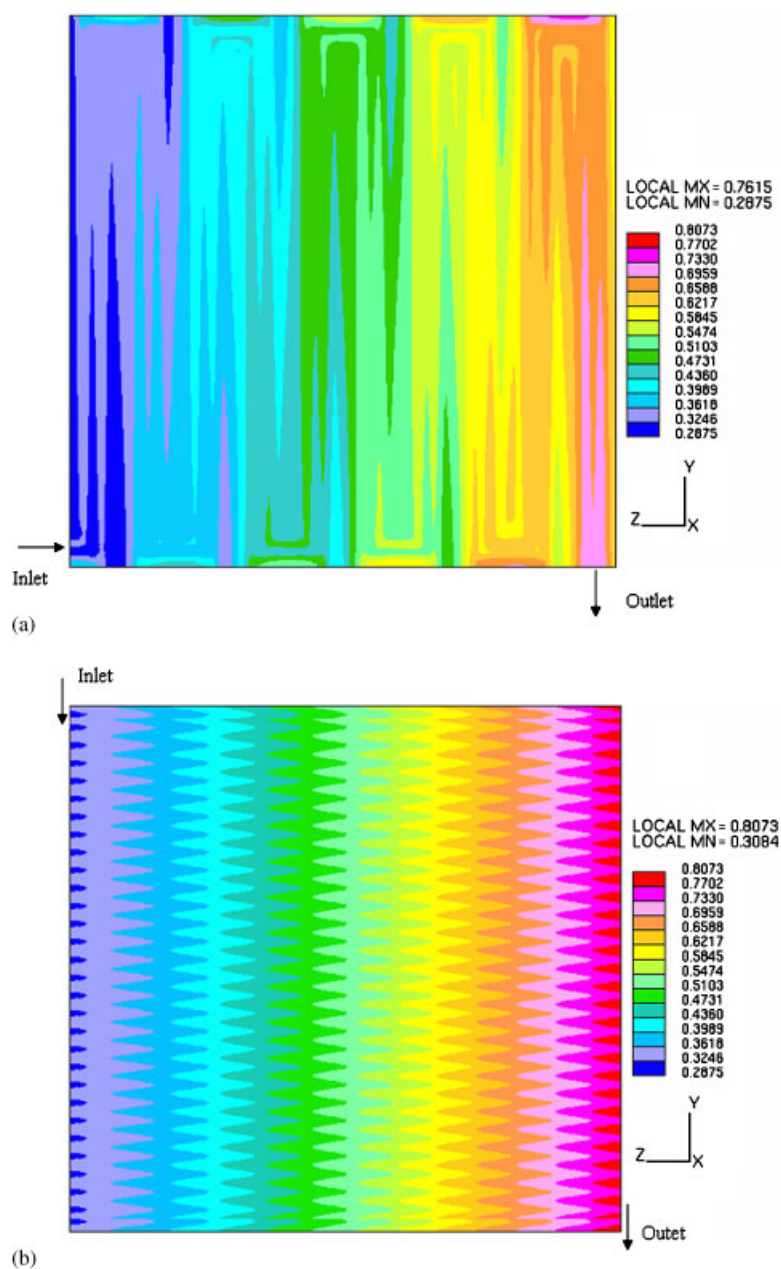


Figure 3. Water activity distributions in the middle section of membrane for: (a) serpentine flow field; and (b) parallel flow field design; for 30% inlet RH at anode and cathode inlet and 0.8 A cm^{-2} average current density.

the membrane is not fully humidified even at this high current density. However, water retention under the U -turns of the serpentine flow field results in water activity greater than unity at these locations.

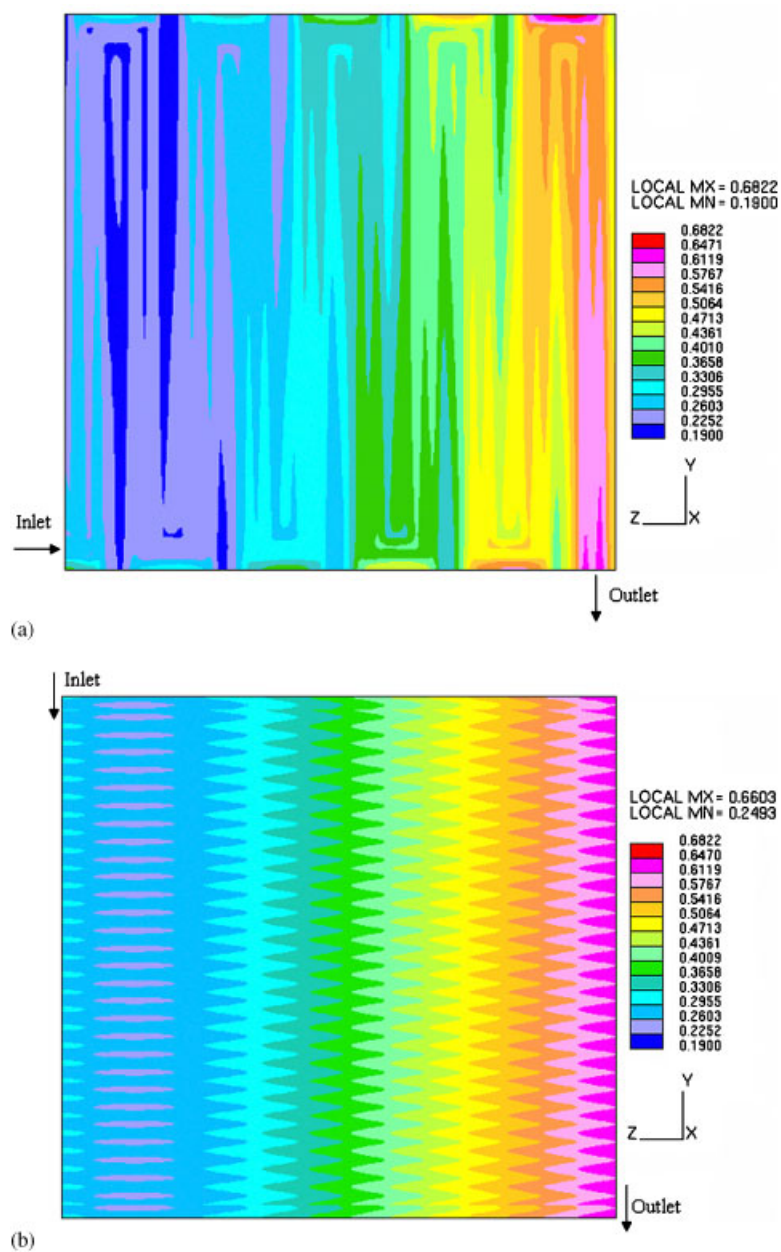


Figure 4. Water activity distributions in the middle section of membrane for: (a) serpentine flow field; and (b) parallel flow field design; for 50% inlet RH at anode and 0% at cathode inlet and 0.8 A cm^{-2} average current density.

Figures 7 and 8, and Figures 9 and 10 show the distributions of ionic conductivity in the middle section of the membrane for the parallel and serpentine flow field designs at 0.8 and 1.6 A cm^{-2} average current densities, respectively. The ionic conductivity depends on

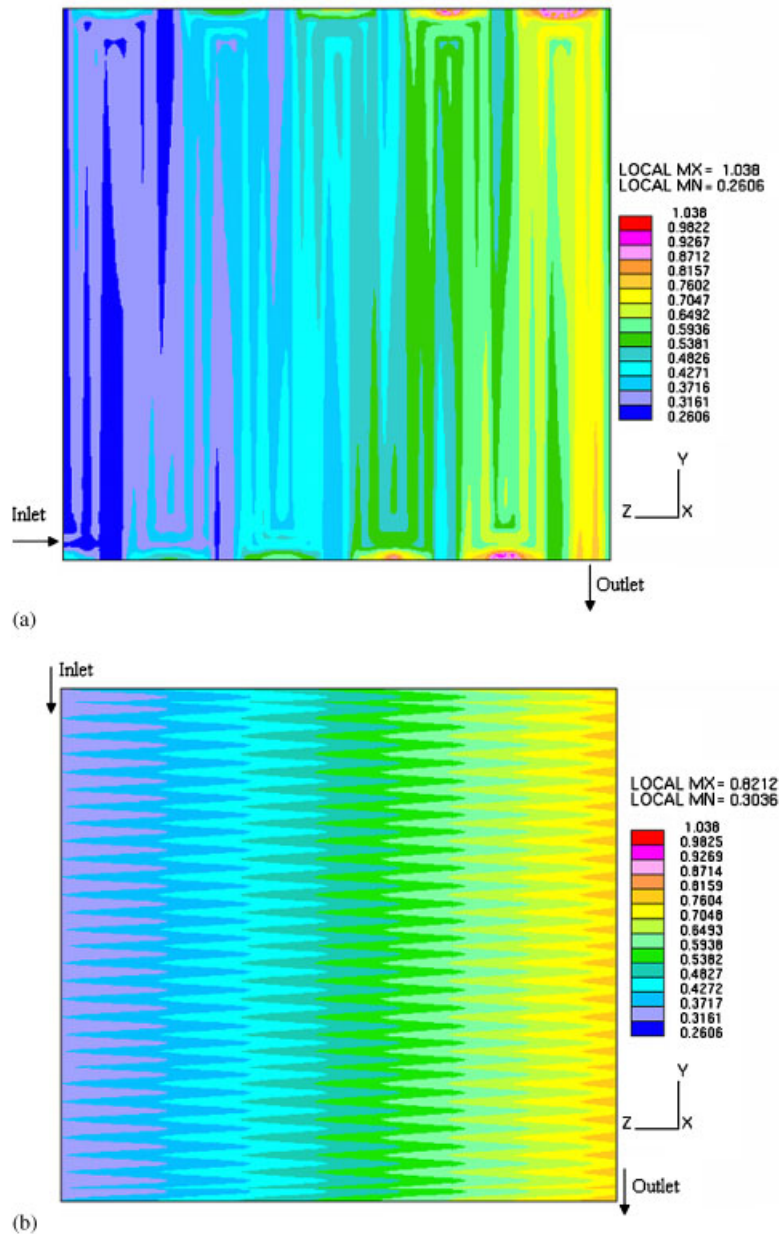


Figure 5. Water activity distributions in the middle section of membrane for: (a) serpentine flow field; and (b) parallel flow field design; for 30% inlet RH at anode and cathode inlet and 1.6 A cm^{-2} average current density.

temperature and water content of the membrane, which in turn is highly influenced by the operating temperature. An increase in the operating temperature results in a significant decrease in the water content of the membrane and, thus, a low ionic conductivity

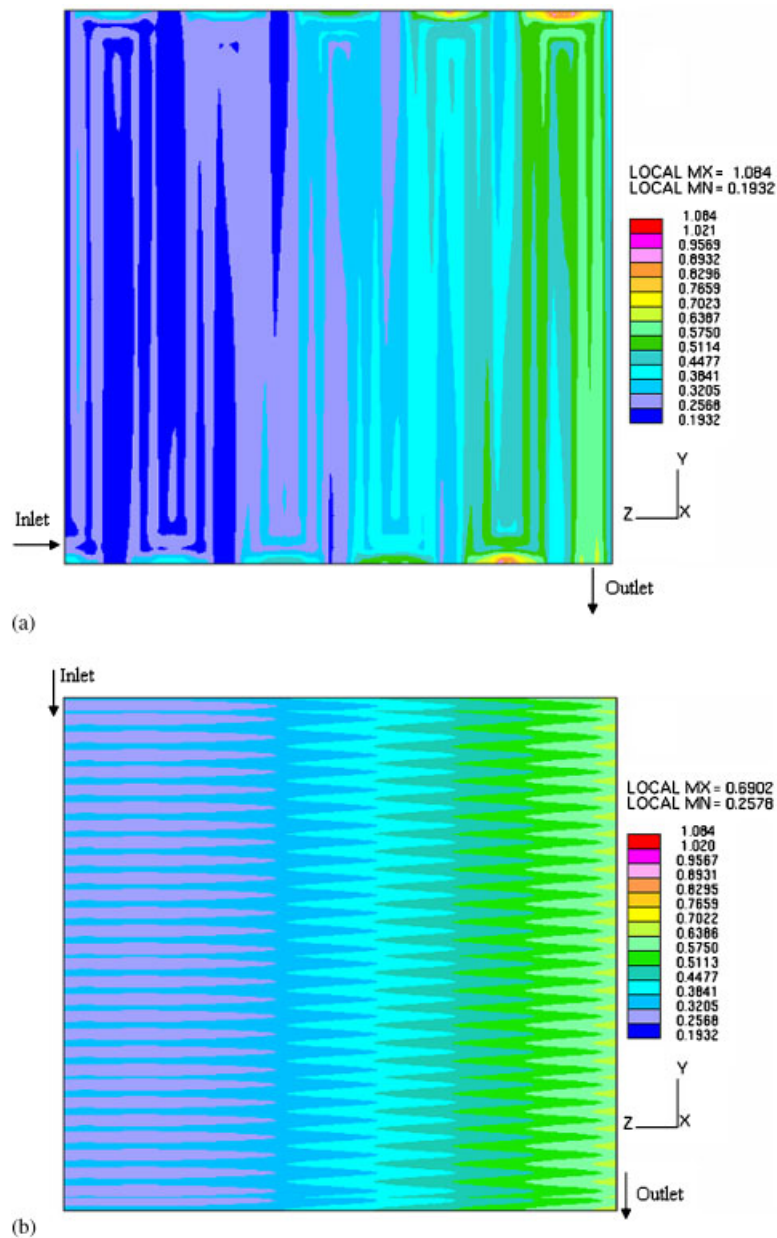


Figure 6. Water activity distributions in the middle section of membrane for: (a) serpentine flow field; and (b) parallel flow field design; for 50% inlet RH at anode and 0% at cathode inlet and 1.6 A cm^{-2} average current density.

of the membrane. For the present work Gore-Select[®] membrane is chosen. The Gore membrane is a microscopically reinforced composite membrane. Due to the reinforcement, the proton conductivity is approximately half of the value of an un-reinforced

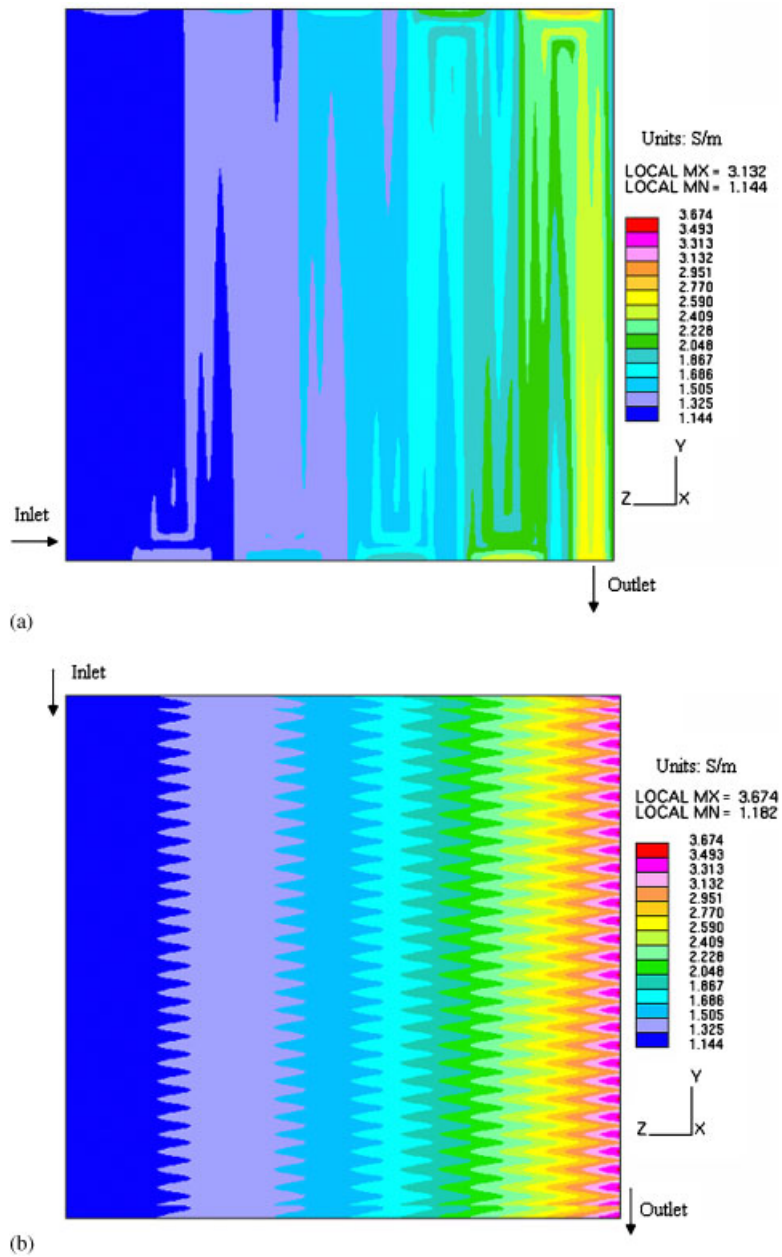


Figure 7. Ionic conductivity distributions in the middle section of membrane for: (a) serpentine flow field; and (b) parallel flow field design; for 30% inlet RH at anode and cathode inlet and 0.8 A cm^{-2} average current density.

membrane (Ju *et al.*, 2005b). As becomes clear from Figures 7–10, the membrane ionic conductivity is well below the fully humidified value and results in large Ohmic overpotential.

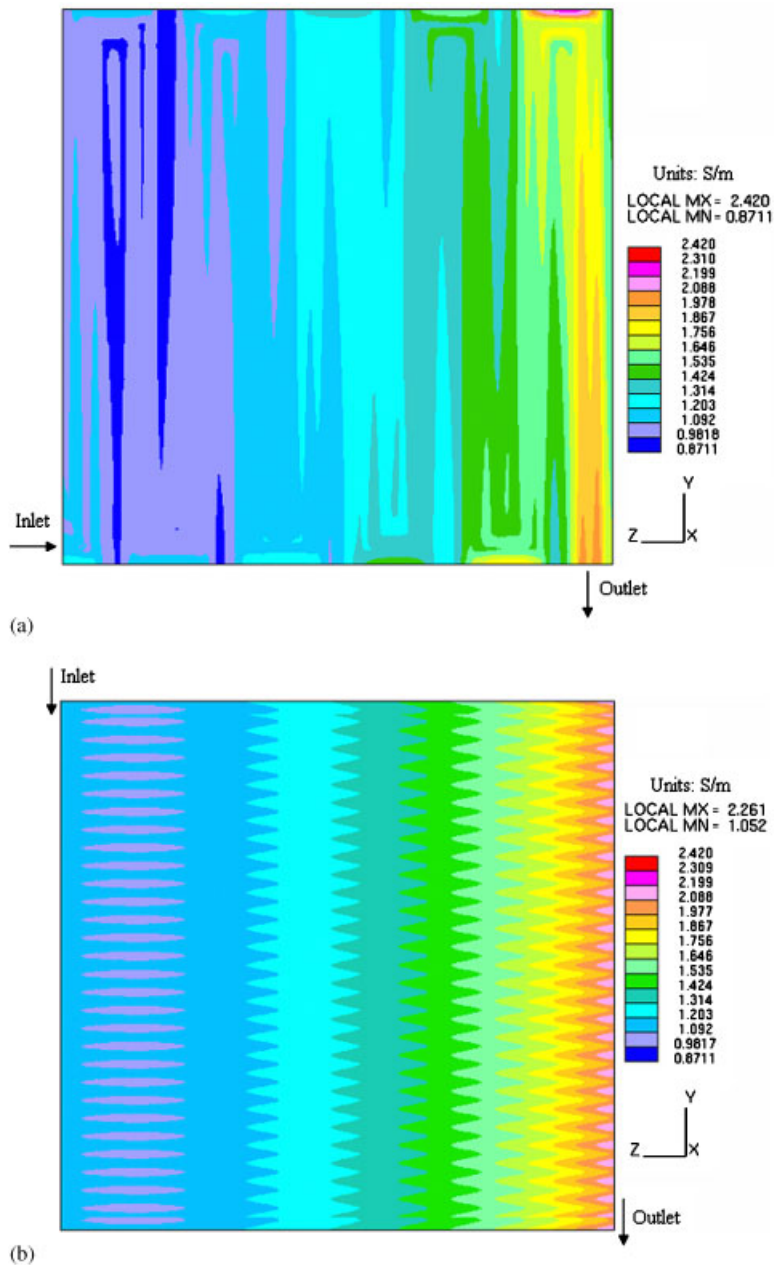


Figure 8. Ionic conductivity distributions in the middle section of membrane for: (a) serpentine flow field; and (b) parallel flow field design; for 50% inlet RH at anode and 0% at cathode inlet and 0.8 A cm^{-2} average current density.

Figures 11 and 12 shows the distributions of current density in the middle section of membrane for parallel and serpentine flow fields at 0.8 A cm^{-2} average current density. The current density is governed by the oxygen concentration in the cathode catalyst

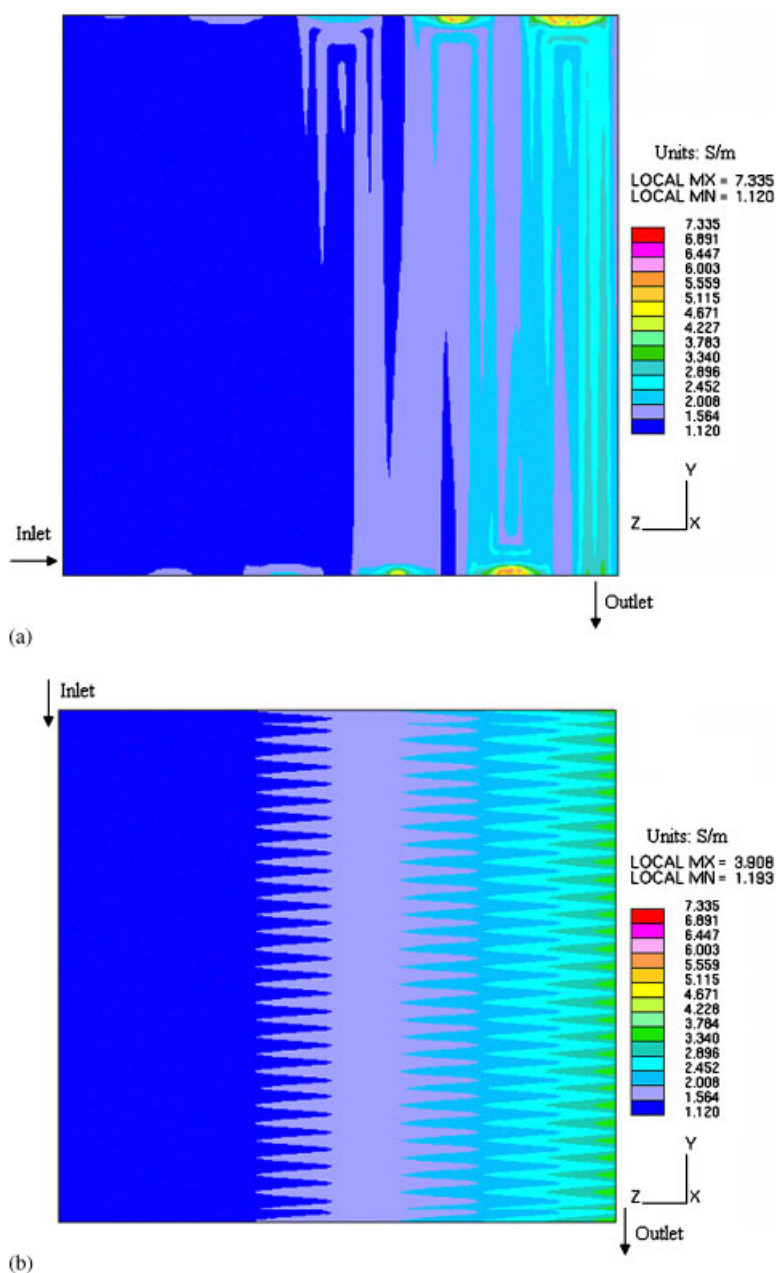


Figure 9. Ionic conductivity distributions in the middle section of membrane for: (a) serpentine flow field; and (b) parallel flow field design; for 30% inlet RH at anode and cathode inlet and 1.6 A cm^{-2} average current density.

layer and the ionic conductivity of the membrane. Over the whole active area, the distribution of ionic conductivity and oxygen concentration in the catalyst layer is more uniform for parallel flow field design, which results in a more uniform distribution of current density.

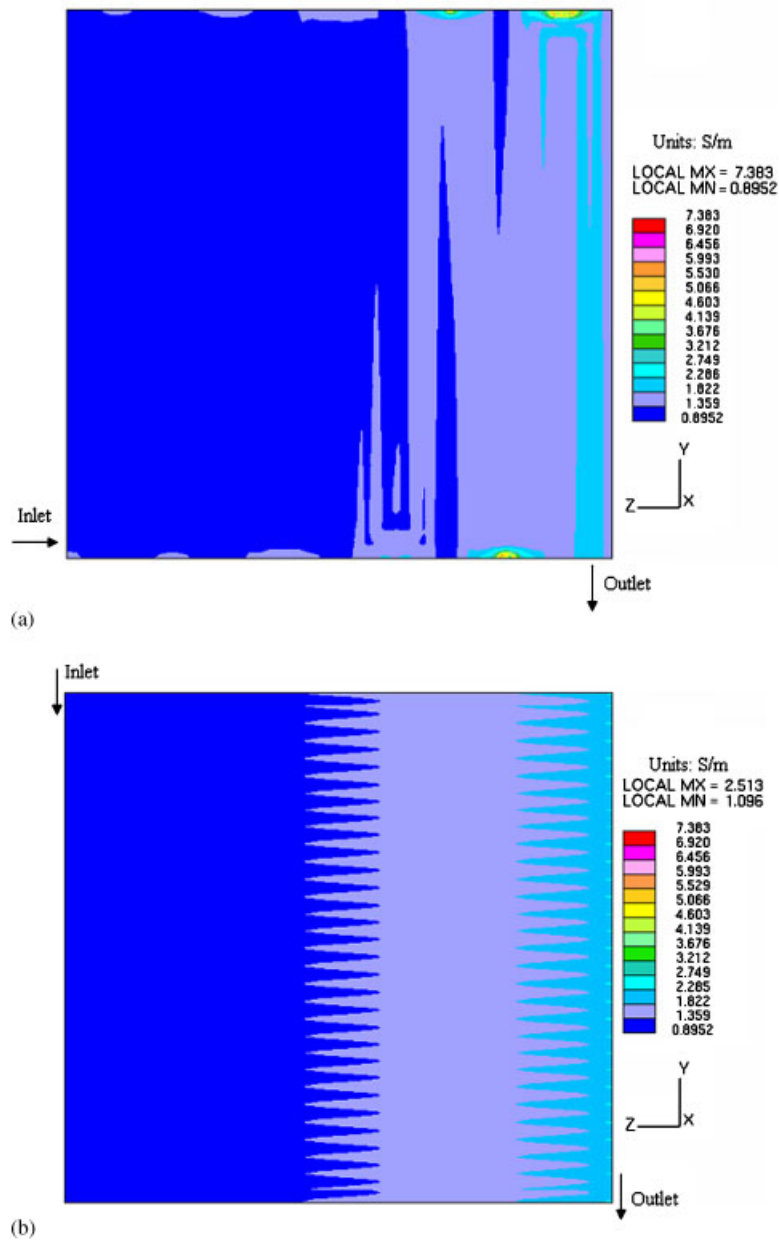


Figure 10. Ionic conductivity distributions in the middle section of membrane for: (a) serpentine flow field; and (b) parallel flow field design; for 50% inlet RH at anode and 0% at cathode inlet and 1.6 A cm^{-2} average current density.

The range over which the current density varies is comparable for serpentine and parallel flow field for 0.8 A cm^{-2} average current density operation. In contrast, the range of the current density distributions differs significantly for 1.6 A cm^{-2} average current density

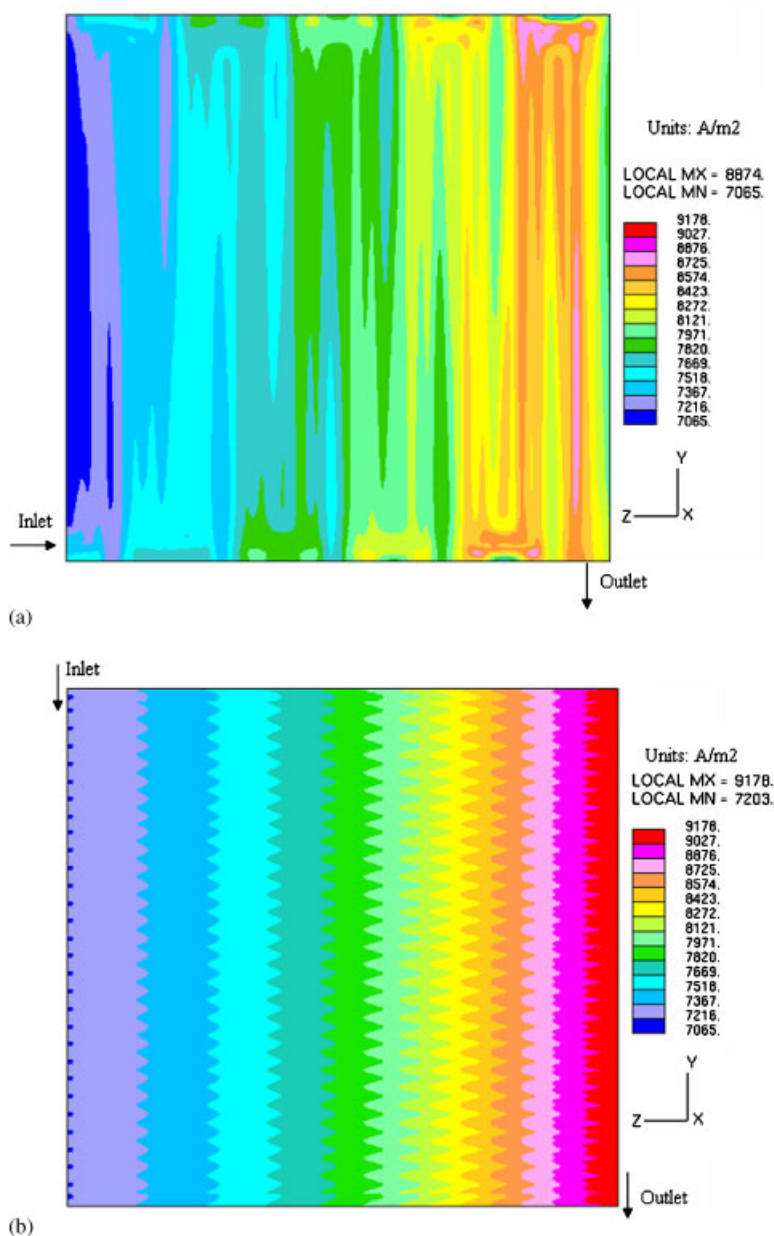


Figure 11. Current density distributions in the middle section of membrane for: (a) serpentine flow field; and (b) parallel flow field design; for 30% inlet RH at anode and cathode inlet and 0.8 A cm^{-2} average current density.

as shown in Figures 13 and 14. With the serpentine flow field and 1.6 A cm^{-2} average current density operation, the current density is very small at the top and bottom edge of membrane and peaks to very high value in close proximity towards the outlet

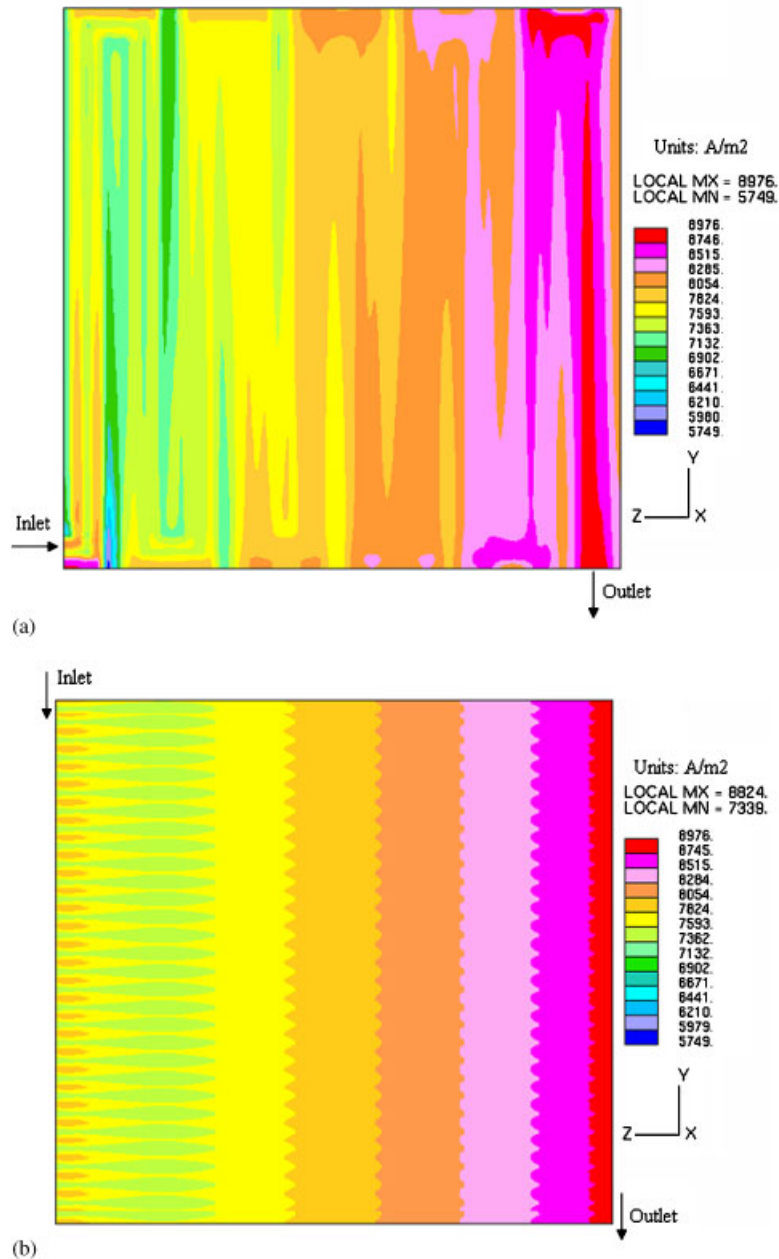


Figure 12. Current density distributions in the middle section of membrane for: (a) serpentine flow field; and (b) parallel flow field design; for 50% inlet RH at anode and 0% at cathode inlet and $0.8 A cm^{-2}$ average current density.

of the gas channels. These areas are shown in Figures 13 and 14 and are called 'dead zones'. The presence of these dead zones may be detrimental for membrane durability.

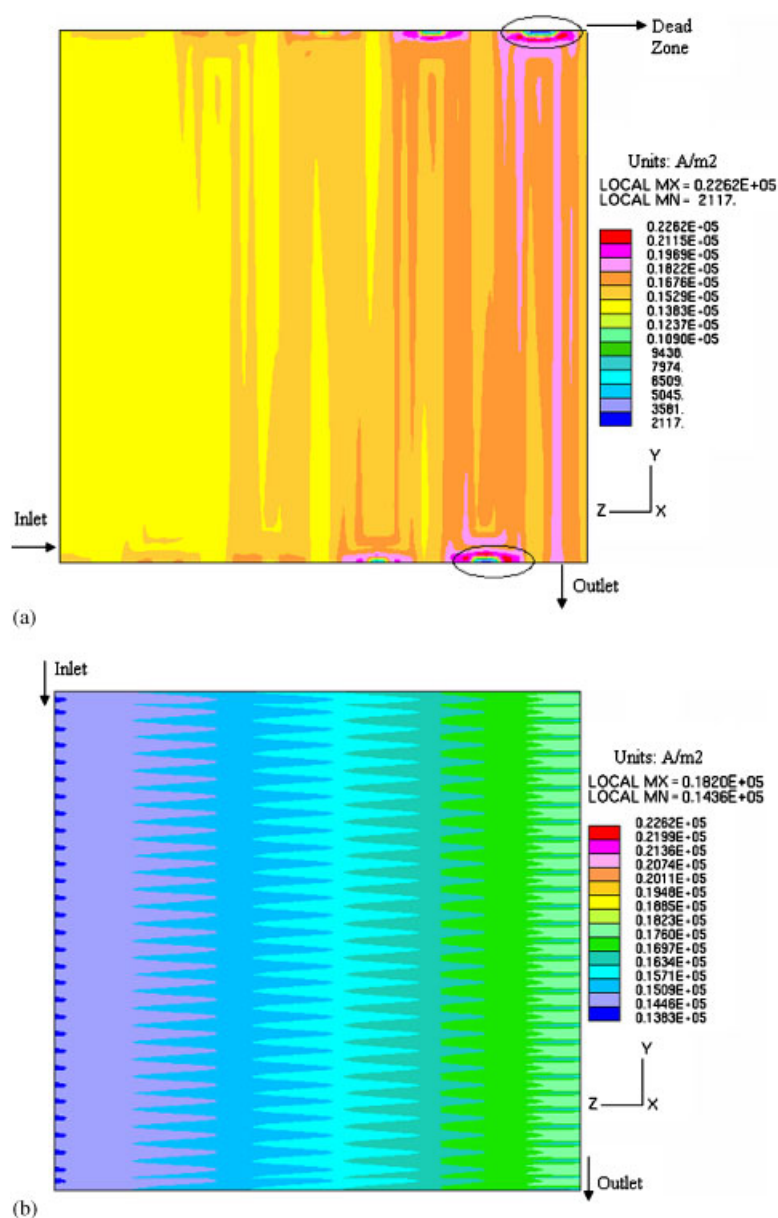


Figure 13. Current density distributions in the middle section of membrane for: (a) serpentine flow field; and (b) parallel flow field design; for 30% inlet RH at anode and cathode inlet and 1.6 A cm^{-2} average current density.

The orientation of the membrane electrode assembly (MEA) and gas diffusion layer (GDL) with respect to the three-pass serpentine flow field is shown in Figure 1(c). As shown in Figure 1(c), the top and bottom edge of MEA lie under the ribs and hence suffer from

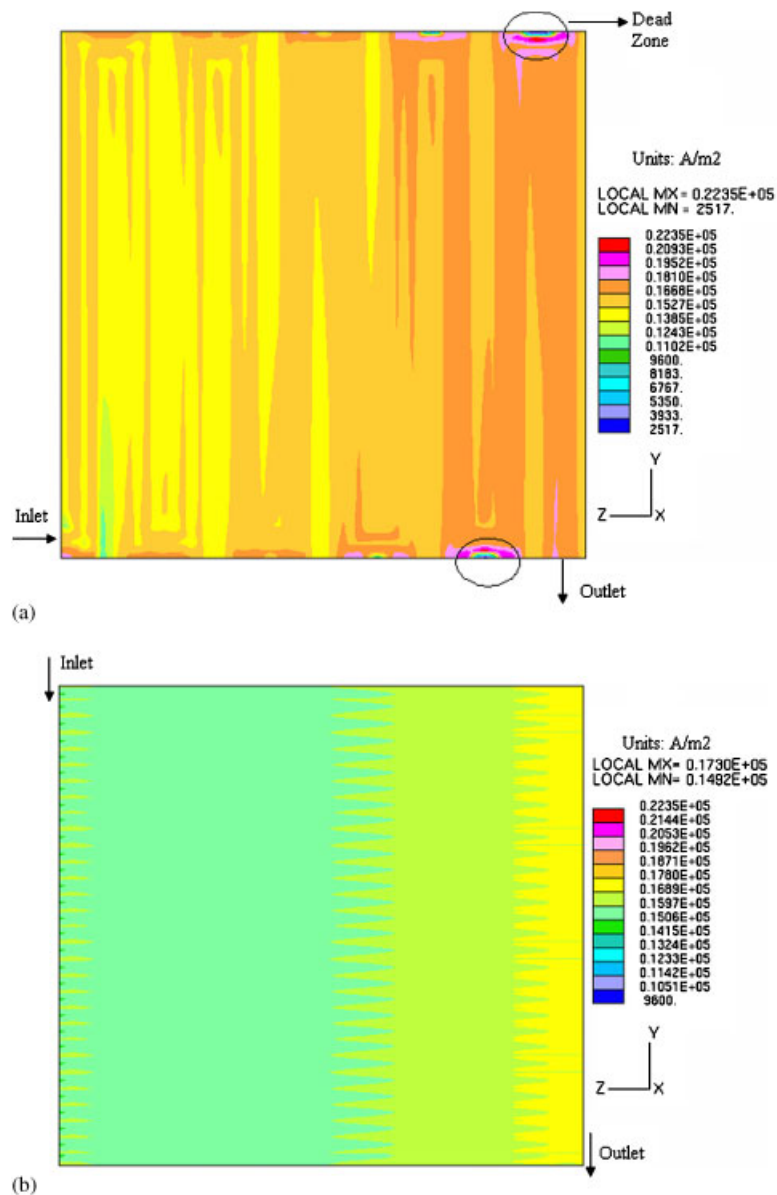


Figure 14. Current density distributions in the middle section of membrane for: (a) serpentine flow field; and (b) parallel flow field design; for 50% inlet RH at anode and 0% at cathode inlet and $1.6 A cm^{-2}$ average current density.

low oxygen concentration. It was shown in an earlier paper (Sinha *et al.*, 2006) that the depletion of oxygen concentration towards the outlet dominates the performance of PEFC at elevated temperatures. As shown here, the depletion of oxygen concentration is more severe for the serpentine flow field compared to the parallel flow field design. Figure 15 shows the distributions of oxygen concentration at the interface of the

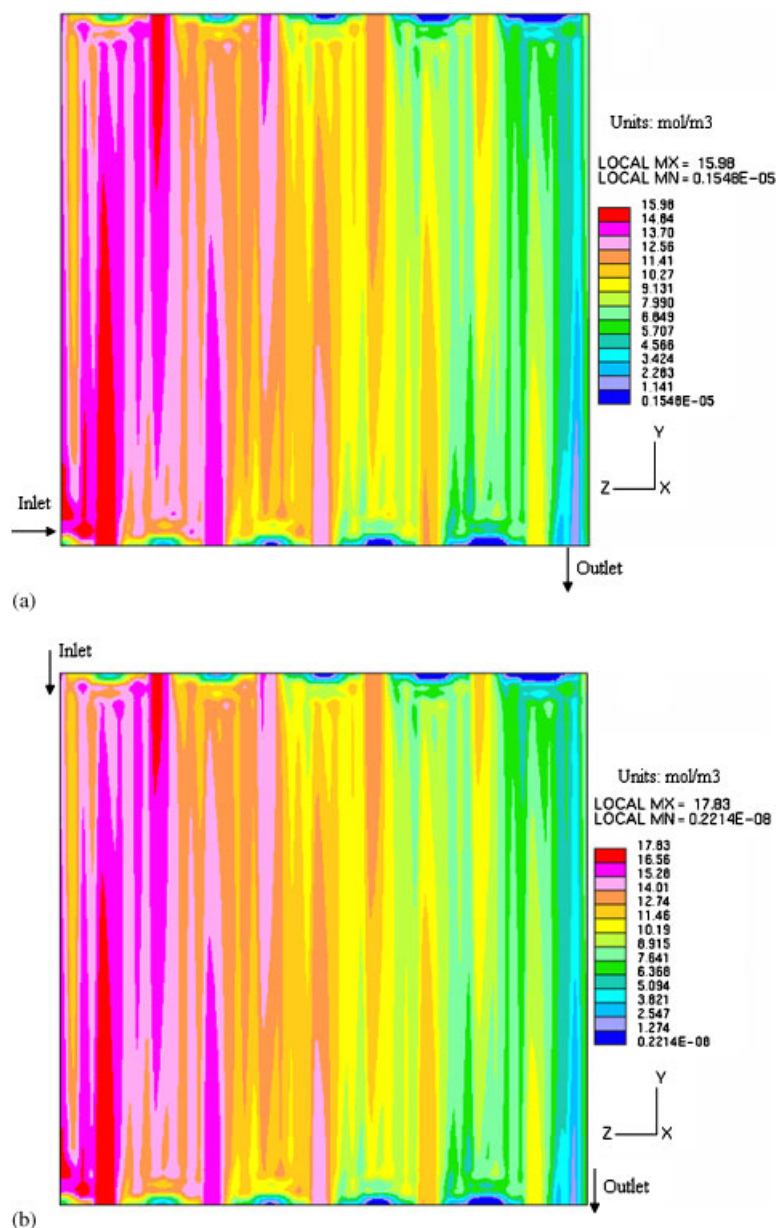


Figure 15. Oxygen concentration distributions at the interface of membrane and cathode catalyst layer with serpentine flow field for: (a) 30% inlet RH at anode and cathode inlet; and (b) 50% inlet RH at anode and 0% at cathode inlet and 1.6 A cm^{-2} average current density.

cathode catalyst layer and membrane for the serpentine flow field design and 1.6 A cm^{-2} average current density operation. As shown in Figure 15, very low oxygen concentration at the top and bottom edges of the membrane towards the outlet causes the occurrence of dead zones.

4. CONCLUSIONS

A three-dimensional single-phase non-isothermal PEFC model was applied to 25 cm² PEFC with two different flow field designs operated with under-humidified feed gas. The main objective of this study was to compare the performance of 25 cm² PEFC operated at 95°C for three-pass serpentine and parallel flow field designs. It was found that the parallel flow field design provides better performance and more uniform distribution of water activity, ionic conductivity, and current density over the active area, which makes it a more favourable design for high-temperature fuel cell applications such as for automobiles. Dead zones were found near the top and bottom edges of the membrane towards the exit of the fuel cell with the serpentine flow field at high current density, which may be detrimental for membrane durability.

NOMENCLATURE

D	= mass diffusivity of species ($\text{m}^2 \text{s}^{-1}$)
EW	= equivalent molecular weight of electrolyte in membrane (kg mol^{-1})
F	= Faraday constant, $96\,487 \text{ C mol}^{-1}$
k	= thermal conductivity (W mK^{-1})
K	= hydraulic permeability (m^2)
p	= pressure (Pa)
R	= the universal gas constant, $8.314 \text{ J mol K}^{-1}$
RH	= relative humidity
T	= temperature (K)

Greek letters

ε	= volume fraction of gaseous phase in porous region
ε_{mc}	= volume fraction of ionomer phase in catalyst layer
ζ	= tortuosity of porous region
ξ	= stoichiometry flow ratio
σ	= electronic conductivity (S m^{-1})

Subscripts

a	= anode
c	= cathode
cat	= catalyst
GDL	= gas diffusion layer
H ₂	= hydrogen
Mem	= membrane
O ₂	= oxygen
Ref	= reference value
w	= water
0	= standard condition, 298.15 K and 101.3 kPa (1 atm)

Superscripts

e	= electrolyte
eff	= effective value in porous region
mem	= membrane
ref	= reference value

ACKNOWLEDGEMENTS

Funding for this work from W.L. Gore & Associates, Inc. is gratefully acknowledged.

REFERENCES

- Bird RB, Stewart WE, Lightfoot EN. 1960. *Transport Phenomena*, Wiley, New York.
- Glandt J, Shimpalee S, Lee W-k, Vanzee JW. 2002. Modeling the effect of flow field design on PEM fuel cell performance. *A.I.Ch.E. Spring National Meeting*, 10–14 March, New Orleans, LA.
- Ju H, Meng H, Wang CY. 2005a. A single-phase non-isothermal model for PEM fuel cells. *International Journal of Heat and Mass Transfer* **48**:1303–1315.
- Ju H, Wang CY, Cleghorn S, Beuscher U. 2005b. Non-isothermal modeling of polymer electrolyte fuel cells. Part I: experimental validation. *Journal of Electrochemical Society* **152**:A1645–A1653.
- Mench MM, Wang CY, Thynell S. 2001. An introduction to fuel cells and related transport phenomena. *International Journal of Transport Phenomena* **3**:151–176.
- Meng H, Wang CY. 2004a. Electron transport in PEFCs. *Journal of Electrochemical Society* **151**:A358–A367.
- Meng H, Wang CY. 2004b. Large-scale simulation of polymer electrolyte fuel cells by parallel computing. *Chemical Engineering Science* **59**:A3331–A3343.
- Pasaogullari U, Wang CY. 2002. Computational fluid dynamics modeling of proton exchange membrane fuel cells. *2002 Fluent Users Groups Meeting*, Manchester, NH.
- Sinha PK, Wang CY, Beuscher U. 2006. Transport phenomena in elevated temperature PEM fuel cells. *Journal of Electrochemical Society*, under review.
- STAR-CD. 2001. STAR-CD version 3.15 Methodology. CD-Adapco Group.
- Springer TE, Zawodzinski TA, Gottesfeld S. 1991. Polymer electrolyte fuel cell model. *Journal of Electrochemical Society* **138**:2334–2342.
- Um S, Wang CY, Chen KS. 2000. Computational fluid dynamics modeling of proton exchange membrane fuel cells. *Journal of Electrochemical Society* **147**:4485–4493.
- Wang CY. 2004. Fundamental models for fuel cell engineering. *Chemical Reviews* **104**:4727–4766.
- Wang Y, Wang CY. 2006. Ultra large-scale simulation of polymer electrolyte fuel cells. *Journal of Power Sources* **153**:130–135.